Indian Journal of Pure & Applied Physics
Vol. 61, March 2023, pp. 165-174
DOI: 10.56042/ijpap.v61i3.70065

Structural, DC Conductivity and Electric Modulus Studies of Polypyrrole Praseodymium Manganite Nanocomposites

Meti Bharathi[a*], K N Anuradha[a] & M V Murugendrappa[b]

[a]Department of Physics, Dr. Ambedkar Institute of Technology, Bengaluru 560 056, India
[b]Centre of Excellence in Advanced Materials Research, Department of Physics, BMS College of Engineering, Bengaluru 560 019, India

Received 3 January 2023; accepted 13 February 2023

Praseodymium Calcium Manganite (PCM) nanoparticles were synthesized by sol-gel method. Polypyrrole (PPy) and polypyrrole–praseodymium manganite nanocomposites (PPy/PCM) were synthesized by in-situ chemical polymerization method. Transmission electron microscope (TEM) confirmed good crystallinity with 42-63 nm average particle size. Scanning electron microscope (SEM) exhibited well-defined core structure of PPy and the PPy/PCM nanocomposites. X-ray diffraction (XRD) patterns of PPy showed amorphous nature and those of composites showed semicrystalline nature. UV-Vis spectroscopy was used to study the energy band gap for all the nanocomposites and hence they may find a place in wide band gap applications. The UV (231nm) and visible (363 nm and 377 nm) emissions were observed from the spectrum. DC conductivity was studied from 473 to 303 K for all the nanocomposites and found that conduction is of semiconductor type. Analysis of electric modulus confirmed the contribution from grain and grain boundary, non-Debye type relaxation and dc conductivity obeyed Correlated Barrier Hopping (CBH) model.

Keywords: Polypyrrole/PraseodymiumManganite; Nanocomposites; DCconductivity; Electric modulus

Introduction

Manganites with perovskite structure of the form $R_x A_{1-x} MnO_3$ where R = Pr, La, Nd, etc trivalent rare-earth ions and A = Ca, Sr, etc divalent alkaline earth ions have attracted intense research. Differently doping with manganites have been investigated by various researchers[1]. Research on the manganites has discovered large magneto-resistance, double exchange, and Jahn-Teller polaron[2]. The inorganic-organic polymer-coated manganites have gained attention due to their magnetic properties and extensive range of applications. Praseodymium oxide is special among rare-earth oxides[3]. Pollert *et al.*,[4] have studied the comprehensive structural study of $Pr_{1-x}Ca_xMnO_3$ by x-ray powder diffraction. Electrically active polymers are known for their high specific capacitance and flexibility[5]. The polypyrrole (PPy) has proved to have good thermal stability, nontoxicity and an easy synthesis method[6,7]. It possesses high electrical conductivity due to its arranged co-planar unique structure assisted by – conjugation interaction[8] which increases the scope of various applications. PPy composites have shown various applications in humidity and gas sensors[9], fuel cells[10], supercapacitors[11], and so on. But few drawbacks like brittleness, inadequate mechanical strength, and poor process ability limits its practical applications[12]. So, to minimize the production cost and improve the overall performance, an effort to synthesize different composites with polypyrrole as host and different nanoparticles of ceramic materials, metal oxides, etc as dopant has been made. Praseodymium oxide nanoparticles have played a vital role in sensor and electronic materials due to the hopping of electrons between the Mn^{+3} and Mn^{+4} states in the lattice[13]. In 1960s Blumstein was the pioneer to prepare such composites of methyl methacrylate with clay who came out with interesting results. This research encouraged lot of work in polymer composites which was reported by Zhang *et al.*[14].

DC current is produced when an electric field applied on the sample drives the charge carriers towards the respective electrode. R. A. Sutar *et al.* studied the effect of Cobalt Aluminum Oxide/PPy nanocomposites on DC Conductivity and showed that there was improvement in the overall conductivity as compared to PPy[15]. Conductivity takes place when thermal energy is utilized by the polarons and bipolarons to hop from filled to vacant states[16,17]. The doped conducting polymers are generally considered

*Corresponding author: (E-mail: metibharathi@gmail.com)

as disordered semiconductors. Rare earth manganite nanoparticles doped to these magnetic semiconductors (conducting polymers), have gained importance as they find applications in various devices like magnetic, humidity and gas sensors and organic semiconductor devices *etc*. The DC electrical conductivity in these nanocomposites can be explained based on the validity of the Band-conduction model for various ranges of temperatures, doping levels, and several variables[18].

In this present work, we report the influence of BCM nanoparticles on morphology and electrical properties of PPy. We made efforts to study the DC conduction mechanism and electric modulus of PPy and PPy/PCM nanocomposites at room and higher temperatures.

Materials and Methods

2.1 Chemicals used

The monomer pyrrole was procured from Chemlabs. Ammonium persulphate (APS) was purchased from Rankem. And praseodymium oxide (Pr_6O_{11}) nanoparticles, absolute ethanol, calcium carbonate, manganese carbonate, ethanol, and conc. HNO_3 were purchased from spectrochem Pvt. Ltd.

2.2 Synthesis

The PPy powder was prepared by the chemical polymerization method. The Sol-gel method was employed to synthesize ($Pr_{0.75}Ca_{0.25}MnO_3$) PCM nanoparticles. The PPy/PCM nanocomposites of different weight percentages (10-50 wt %) were synthesized by the in-situ chemical polymerization method[19] as explained in our previous paper.

2.3 Characterization

TEM and SAED were performed by JEOL/JEM 2100 TEM, Cochin. TESCAN Vega 3 SEM was used to study the morphology of the samples. The size of the particles was measured by ImageJ software. XRD analysis was carried out using Rigaku Ultima-IV model diffractometer with 2θ from 10° to 80°. The absorption spectra of all the samples were recorded by Agilent Cary 5000 UV-Vis NIR Spectrophotometer, STIC, Kochi. The optical reflectance was measured in the range of 200-800 nm. DC conductivity was measured using Keithley Apparatus from 473K to 303K. AC conductivity was measured by Wayne Kerr Impedance analyser 6500B in the temperature range 303–453K in the frequency range 100 Hz–1 MHz.

3 Results and Discussions

3.1 TEM and FESEM Analysis

TEM micrographs of PPy, PCM and PPy/PCM nanocomposites shown in Fig. 1 indicates agglomeration of non-uniformly sized particles with spherical structures. On an average, the size of PCM nanoparticles was in the range 35-60 nm. PCM nanoparticles are evenly spread in the polypyrrole rings without agglomeration. The HRTEM micrographs with (inset) SAED patterns for PPy and

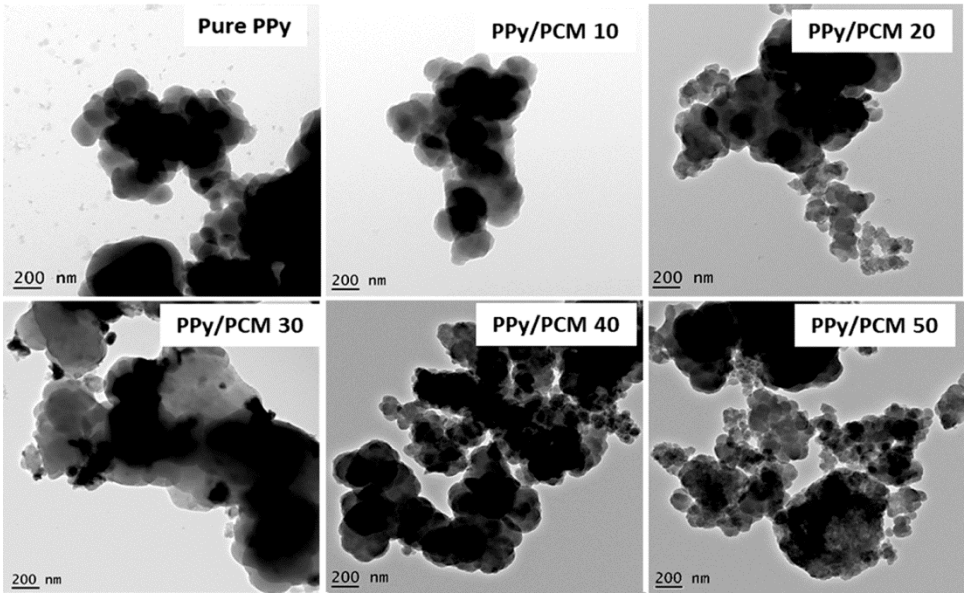

Fig. 1 — TEM micrographs for PPy and PCM/PPy nanocomposites.

PCM/PPy composites shown in Fig. 2 reveals dark patches which confirms the presence of PCM in the PPy matrix. The interplanar distance (d) being 0.26 nm matches well with the spectrum of XRD with diffraction plane (002) seen in Fig. 5(b). The formation of PPy/PCM nanocomposites has been confirmed. SAED patterns confirm polycrystalline nature of the composites. Due to the high crystallinity bright spots were detected in the diffraction pattern in SAED.

Figure 3 shows the SEM micrographs of pure PPy and 10 to 50 wt % of PPy/PCM nanocomposites respectively. Clusters of PCM nanoparticles are observed to be agglomerated and PPy shows granular structure. The PPy/PCM nanocomposites are found to show clusters of PCM embedded in PPy chain. Histograms shown in Fig. 4 gives the distribution of particle size. ImageJ software was employed to evaluate the average particle size.

The average size of PPy, PCM/PPy and PCM nanoparticles are listed in Table 1. The size of PPy is found to be in the range of 500-570 nm. There was increase in size of the nanocompositesas the weight percent of PCM in PPy increased. This may be due to the rise in the nucleation sites during the process of chemical polymerisation of PPy.

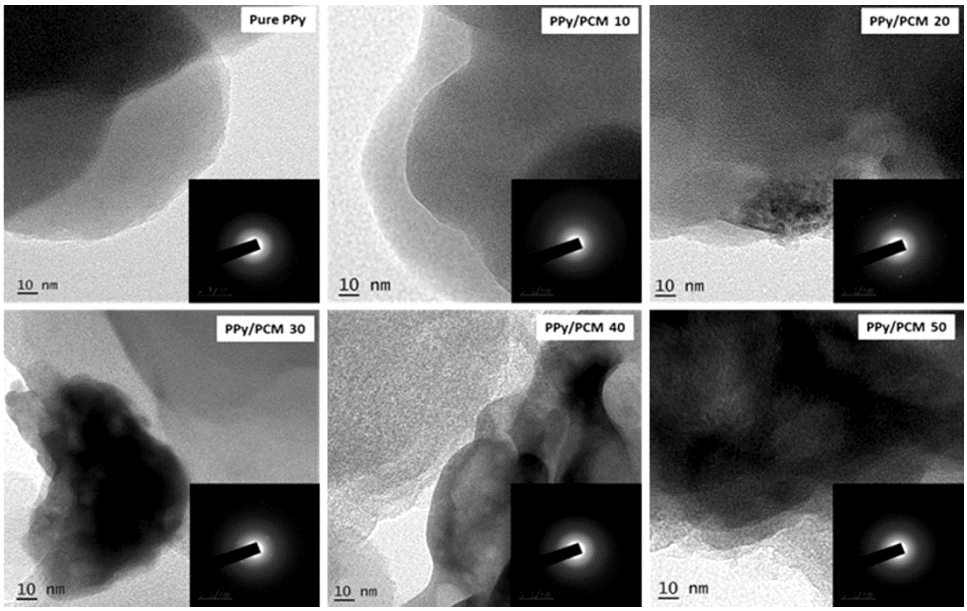

Fig. 2 — HRTEM micrographswithinset SAED patterns for PPy and PCM/PPy nanocomposites.

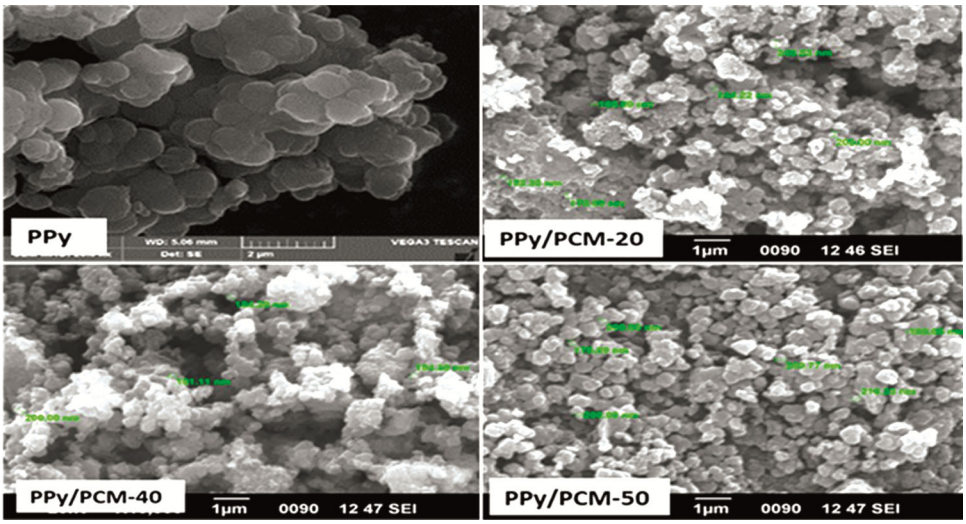

Fig. 3 — FESEM micrographs of PPy, and PPy /PCM nanocomposites.

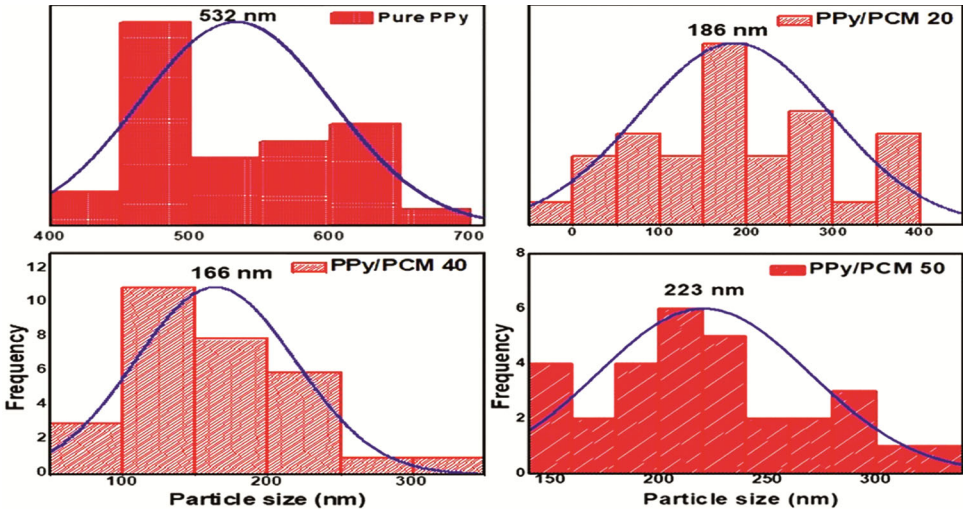

Fig. 4 — Histograms of PPy, and PPy /PCM nanocomposites.

Table 1 — The average size of PPy, PCM/PPy and PCM nanoparticles

Composites	Particle size (nm)
PPy	532
PPy/PCM-10	196
PPy/PCM-20	186
PPy/PCM-30	205
PPy/PCM-40	166
PPy/PCM-50	213
PCM	42

3.2 XRD Analysis

Rietveld's refinement of the XRD pattern of PCM nanoparticles is seen in Fig. 5(a). The lattice constants were found to be a=5.40428Å, b=7.61275 Å and c= 5.39414Å with cell volume 221.21Å^3. The PCM nanoparticles exhibits crystal structure of orthorhombic perovskite with space group Pnma. The peak positions match well with the JCPDS card no. 89-795.Fig. 5 (b) shows the stacked XRD pattern of pure PCM nanoparticles, pure PPy, and all PPy/PCM composites. The broad peak at 2θ = 25° confirms amorphous nature of PPy in the XRD pattern[20]. This peak broadening can be attributed to PPy chain scattering at the inter planner spacing (d)[21]. The d value of 0.26 nm has matched well with the XRD spectrum for the diffraction plane (002) as presented in Fig. 5(a). This confirms the PPy/PCM nanocomposites being formed. The average of crystallite size of PCM was calculated to be 40-63 nm. Average crystallite size and % crystallinity of pure PCM and PPy/PCM nanocomposites is given in Table 2.

3.3 UV-Vis Spectroscopy

UV-VIS absorption spectrums for PPy and all nanocomposites are shown in Fig. 6(a). A characteristic

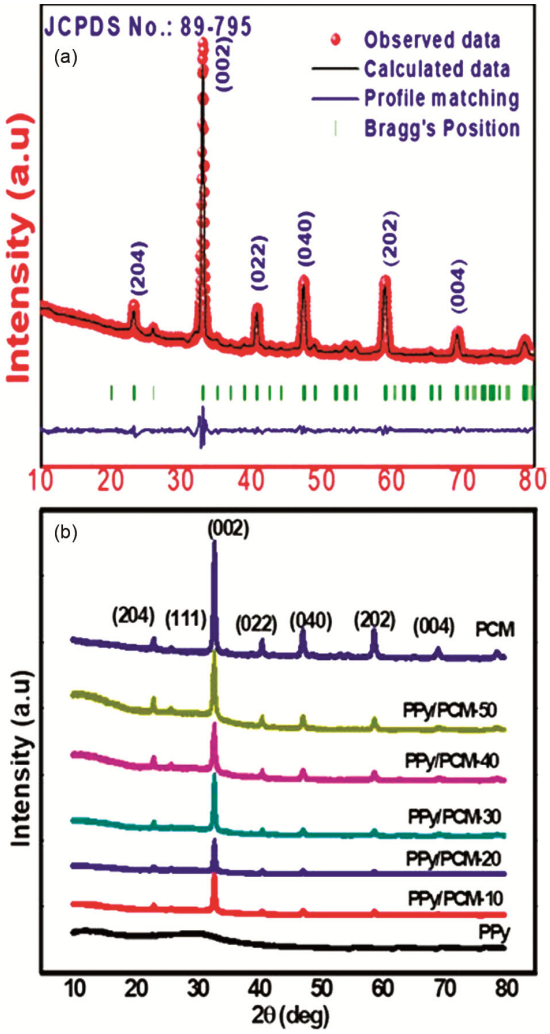

Fig. 5 — (a) Reitveld refinement of XRD pattern of PCM nanoparticles and (b) XRD pattern of pure PCM nanoparticles, pure PPy and PPy/PCM nanocomposites.

Table 2 — Average Crystallite size and % Crystallinity of pure PCM and PPy/PCM nanocomposites

Material	Average Crystallite size nm		Crystallinity%
	Scherrer's formula	W-H plot	
PCM	14.36	12.47	74
PPy/PCM-10	26.46	29.60	48
PPy/PCM-20	28.65	31.37	51
PPy/PCM-30	27.12	33.62	55
PPy/PCM-40	29.09	35.38	67
PPy/PCM-50	29.87	31.54	71

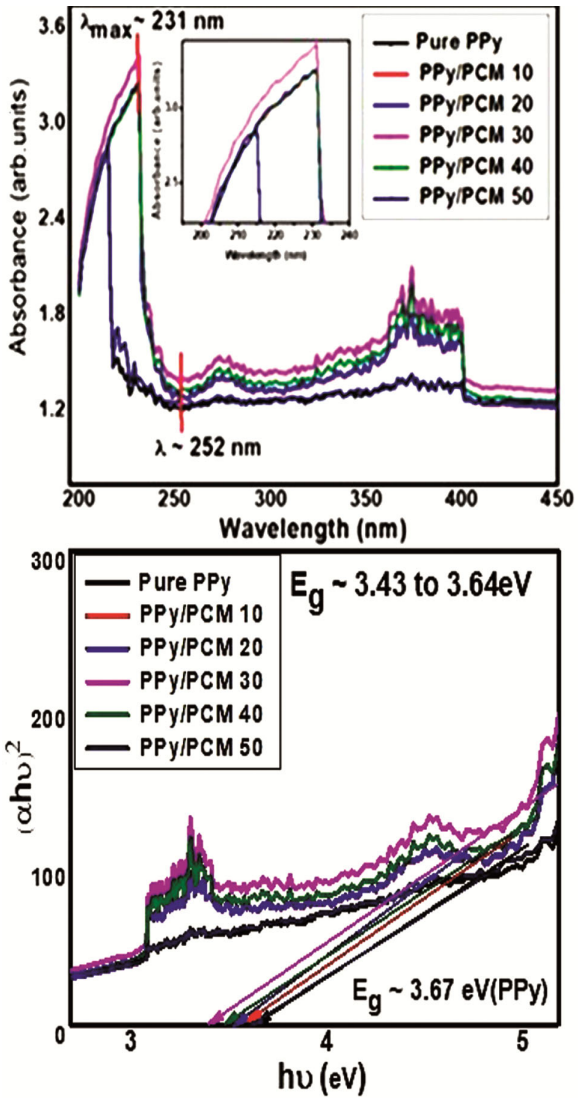

Fig. 6 — (a) UV-Vis absorbance versus wavelength graph and(b)Tauc's plot of $[\alpha h\nu]^2$ vs hν of PPy and PPy/PCM composites.

peak shown by the absorption band in the range of 220-240 nm signifies that PPy is formed. And the hump in the absorption spectrum of polypyrrole in the 250-300 nm range attributes to the transition of bipolarons in the polymer. The peak values in the absorption band vary depending on the chemical structure, morphology and counter ions of the polymer[22]. The energy gap of pure polypyrrole and its composites are evaluated using the Tauc's equation[23] given by

$$(\alpha h\nu)^2 \propto (h\nu - E_g) \quad \ldots (1)$$

Where hν is the energy of photon, α is the coefficient of Absorption and E_g is bandgap.

A graph with $(\alpha h\nu)^2$versus hν was plotted to compare the E_g of pure PPy and PPy/PCM nanocomposites as shown in Fig. 6(b). The band gap of pure polypyrrole is observed to be higher than that of all the composites. This decrease in the band gap in the PPy/PCM nanocomposites is due to the shift in the valence and conduction bands[24]. The absorption spectrum of PPy shows two distinct characteristic peaks; a prominent one at 220 nm, which corresponds to the valence to conduction ($\pi - \pi^*$) band transition of aromatic C=C, and the second absorbance at around 275 nm that is correlated to the bipolaronic band transitions[25].

Table 3 — The optical bandgap for PPy and PPy/PCM composites

Composites	Energy gap (eV)
PPy	3.67
PPy/PCM-10	3.47
PPy/PCM-20	3.43
PPy/PCM-30	3.45
PPy/PCM-40	3.54
PPy/PCM-50	3.64

The bandgap values are calculated using the Kubelka-Munk (K-M) method, and the values are tabulated in Table 3. After the isosbestic point, the absorption shows a slight red-shift due to the addition of PCM nanoparticles into the PPy matrix. Hence, a slight reduction in the bandgap is witnessed for the nanocomposites. The variation in the band gap is attributed as quantum mechanical effect referred to as quantum confinement. The transitions are between Highest Occupied Molecular orbital (HOMO) to the Lowest Unoccupied Molecular Orbital (LUMO)[26] of the constituent conjugated polymers (PPy) with that of the dopant (PCM nanoparticles).

3.3 DC Conductivity

The expression for DC conductivity is given by,

$$\sigma_{DC} = \frac{RL}{A} \quad \ldots (2)$$

where R is the resistance of the material in ohms, L, the thickness of the material in mm and A being the area of the pellet in mm^2.

The pellets varying with thickness of 1mm-2mm were used for the DC conductivity studies. The D.C.

conductivity was studied in the 473-303 K temperature range. Fig. 7 shows variation of DC conductivity of PPy and PPy/PCM nanocomposites with temperature. It is clear that for the PPy/PCM nanocomposit, the DC conductivity value is directly proportional to temperature. Based on the Band-conduction model, initially the conduction is slow at low temperatures which gradually increases due to the enhancement in the weakened bonds of the grains that enhances the conductivity of charge carriers through the grain boundaries. Hence, higher is the temperature, greater is the DC conductivity. This suggests that PPy/PCM composites behave like a semiconductor material. The

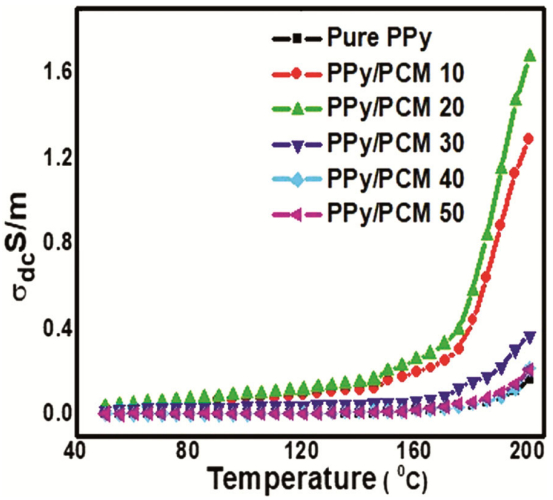

Fig. 7 — DC Conductivity as a function of Temperature for pure PPy and PPy/PCM nanocomposites.

conductivity is seen to be maximum for PPy/PCM 20 wt.%. This is the percolation threshold for these composites. From TEM and FESEM micrographs it was seen that the PPy bulk particles encapsulate the PCM nanoparticles and hence, the particle size reduces and the compactness increases enhancing the conductivity. Hence, the dimensions of nanoparticles in the PPy matrix influence the conductivity.

3.5 Activation Energy: Determination from Arrhenius Equation

The minimum amount of energy that must be provided to initiate a reaction is Activation Energy. Activation energy (E_a) and rate constant (k) are related by the Arrhenius equation as

$$k = Ae^{-E_a / RT} \quad \ldots (3)$$

where R is the Rydberg constant (R=8.3145 J/K mol), T is absolute temperature (K) and A is pre-exponential factor. Fig. 8 shows Arrhenius plots of PPy and PPy/PCM nanocomposites. All the curves are linearly fitted. The Activation energies of PPy and PPy/PCM nanocomposites are tabulated in the Table 4. The activation energy for PPy/PCM 20 is observed to be minimum hence showing maximum conductivity. For higher weight percent, conductivity has decreased due to excessive accumulation of PCM particles in PPy matrix which blocks the conduction path[27]. The enhanced value of E_a for PPy/PCM 40 may be because bipolaronic band separation is wider[28]. For higher weight percent of PCM in PPy, the activation energy enhances due to the creation of

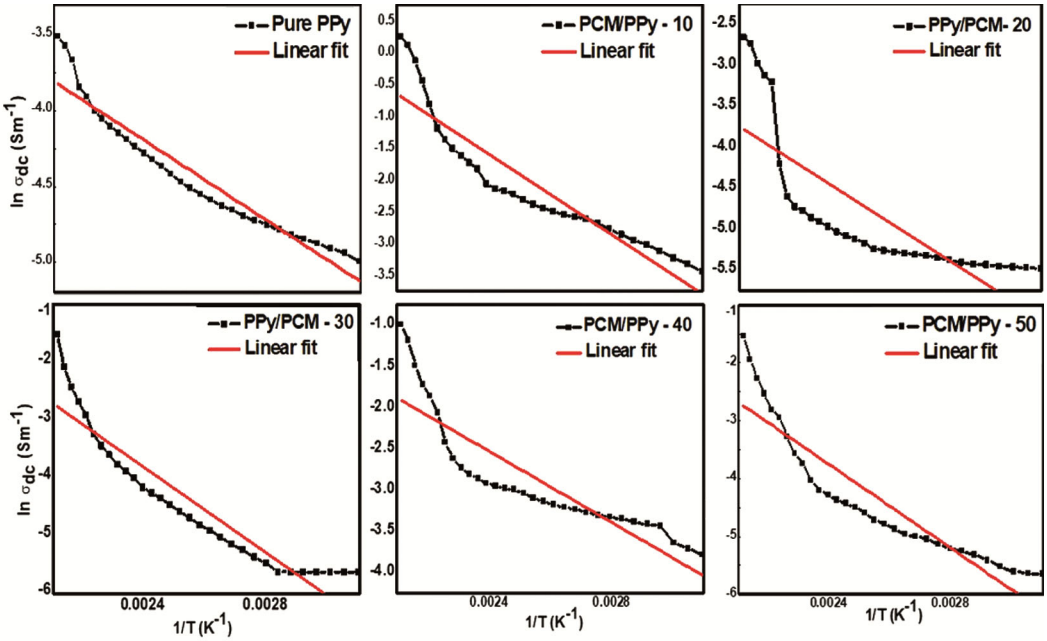

Fig. 8 — Arrhenius plots of DC conductivity of Pure PPy and PPy/PCM composites.

Table 4 — Activation energies of pure PPy and PPy/PCM nanocomposites DC Conductivity

Material	Activation energy in eV
Pure PPy	0.113752
PPy/PCM-10	0.141569
PPy/PCM-20	0.103019
PPy/PCM-30	0.199861
PPy/PCM-40	0.286138
PPy/PCM-50	0.261028

higher potential barrier in the pathway of bipolarons. DC conductivity is not only a function of temperature but also dielectric constant[29]. Hence E_a does not always increase with an increase in weight percent.

3.6 Electric Modulus Studies

Electric modulus (M^*) is given as the inverse of complex permittivity. The PCM when doped with polymers gives rise to interfacial polarisation leading to heterogeneous materials. Electric field relaxation in these conjugated polymers results in short range AC and long-range DC conductivities. From impedance studies it is not possible to differentiate the resistance of grains and grain boundaries. Hence, the grain effects will be magnified in electric modulus explanation given by Macedo *et al.*[30]. The complex electric modulus (M^*) is defined by the equation,

$$M^* = M' + jM'' \quad \ldots (4)$$

where M' and M" are the real and imaginary parts of the electric modulus.

The complex electric modulus studies clearly explain whether the electrode or the defects contributes for conductivity and dielectric properties of the nanocomposites. It represents the relaxation of the electric field in the compound. Real electric modulus M′ is given by

$$M' = \frac{\varepsilon'}{\varepsilon'^2+\varepsilon''^2} \quad \ldots (5)$$

Where ε′ and ε″ are real and imaginary parts of dielectric constant given by, $\varepsilon'' = \varepsilon' \tan\delta$.

Figure 9 shows real (M') and imaginary part (M") of electric modulus as a function of frequency for PPy and PPy/PCM composites at 303K. Initially at low-frequencies M′ shows very low values, then it increases with frequency upto 1 MHz to a maximum value, and then saturates beyond 1 MHz. This is attributed to the long range mobility charge carriers and electrode polarization effect (31, 32) which decreases at high frequency. The electric modulus increased beyond 10^5 Hz due to the charge carriers in motion[33].

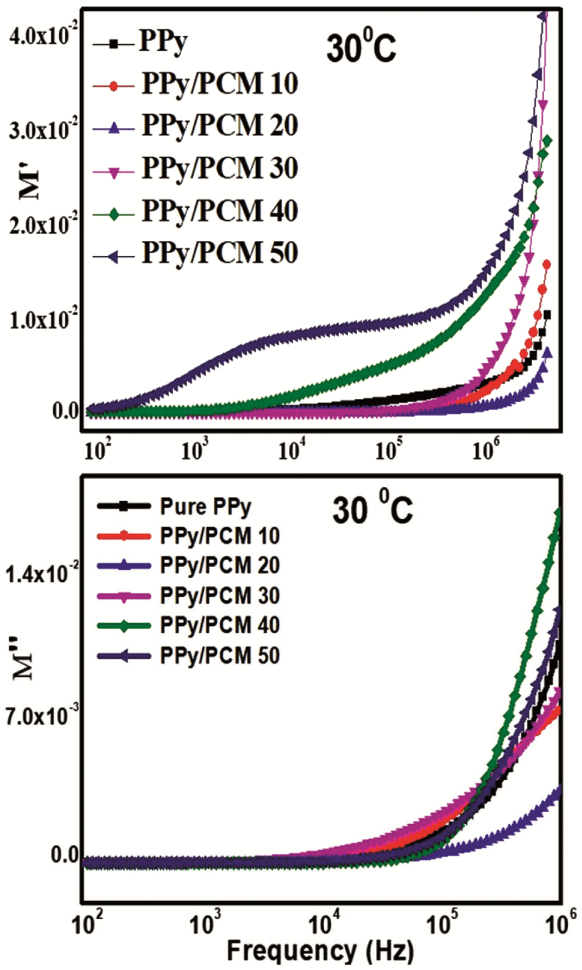

Fig. 9 — Real and Imaginary part of electric modulus as a function of frequency for pure PPy and PPy/PCM nanocomposites at 303K.

The nanocomposite PPy/PCM 20 showed least value of M′ as the composite is feasible for the movement of charge carriers. As M′ changes there is variation in the stiffness of the material which is shown as loss peak in M″ graph. Imaginary electrical conductivity M″ is given by

$$M'' = \frac{\varepsilon''}{\varepsilon'^2+\varepsilon''^2} \quad \ldots (6)$$

The notations are as explained earlier.

Figures 10 & 11 show variation of real(M') and imaginary part (M") of electric modulus as a function of frequency for PPy and PPy/PCM composites from 303 to 453K. The PPy/PCM 50 shows two broad peaks, one in the frequency range of 10^3-10^4 Hz and the other beyond 10^6 Hz, confirm the grain boundary and also grain relaxation. The broad relaxation could be due to overlapping of relaxation frequencies of grain boundaries of PPy-PPy and PPy-PCM interface.

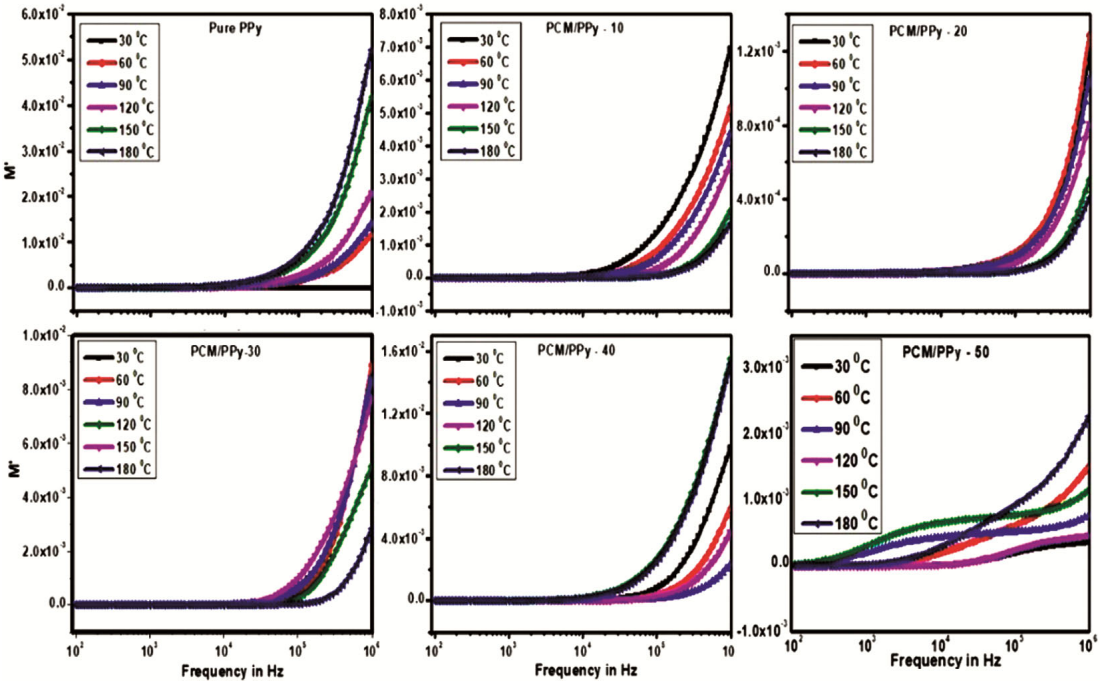

Fig. 10 — Temperature-dependent Real part (M') of electric modulus as a function of frequency for PPy and PPy/PCM composites.

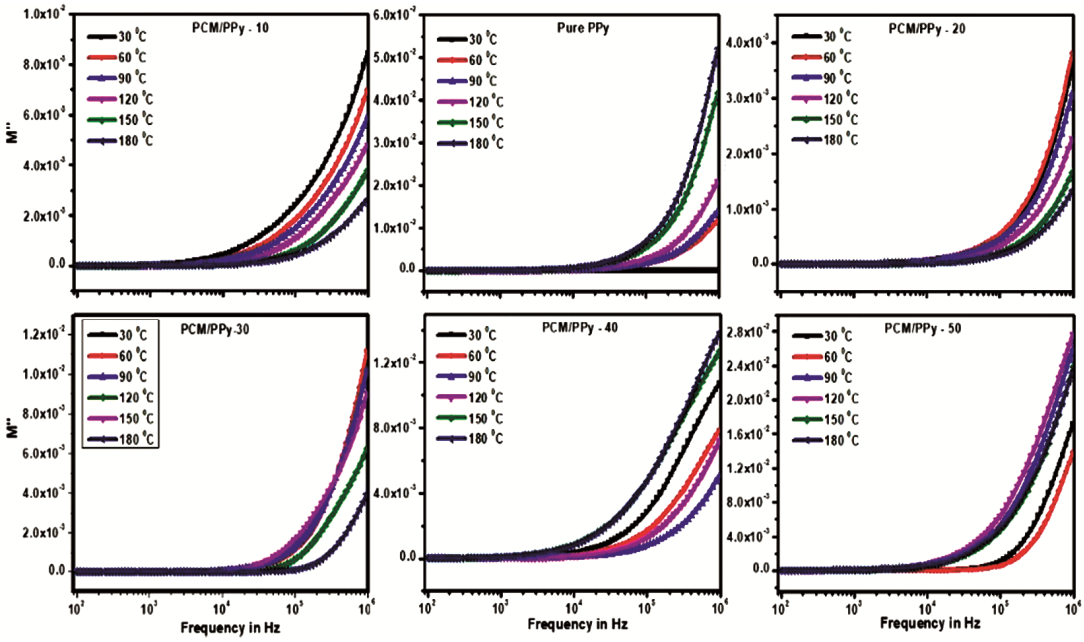

Fig. 11 — Temperature-dependent imaginary part (M") of electric modulus as a function of frequency for PPy and PPy/PCM composites.

This is a non Debye type of relaxation. In Comparison with PPy, all nanocomposites, except PPy/PCM 20, showed less values of bulk resistance and dielectric loss. The M' and M″ decreases with increasing temperatures showing that there is decrease in overall polarization which enhances charge carriers. And PPy/PCM 40 showed the highest M' and M″ values which confirms that polarization is dominant and hence shows least conductivity. The relaxation peak due to grain boundaries shifts towards higher frequencies (beyond 1MHz). As the charge carrier mobility increases with temperature, the accumulation of charge carriers at the grain boundaries diminishes with a decrease in relaxation time.

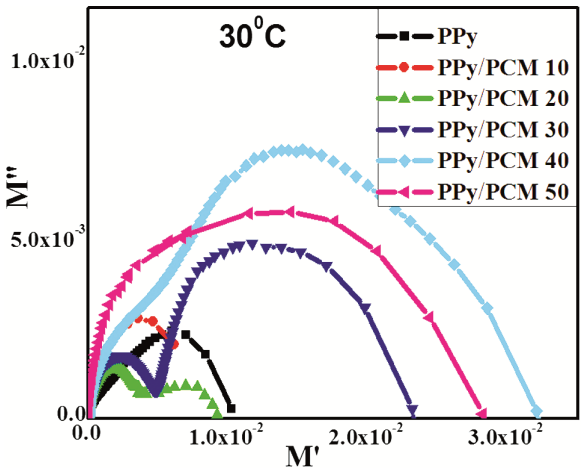

Fig. 12 — Nyquist plot M′ versus M″ of PPy and PPy/PCM nanocomposites at 303K.

3.7 Nyquist Plot of Electric Modulus of PPy/PCM Nanocomposites

Figure 12 shows (Cole–Cole) Nyquist plot of electric modulus of PPy and PPy/PCM composites (M′ versus M″plot) at 303K. The PPy, PPy/PCM 10 and PPy/PCM 40 and PPy/PCM 50 samples showed single arc which characterizes lone phase of the composites. The asymmetric arc confirms single relaxation[34,35]. And the PPy/PCM 20 and PPy/PCM 30 nanocomposites showed two semicircles-one at the higher frequencies corresponding to the grain influence[36] and the other at the lower frequencies corresponding to the effect of grain boundary. Hence, these offer high resistance to the mobility of the charge carriers reducing their conductivity.

3 Conclusions

The synthesized PCM nanoparticles, PPy and PPy/PCM nanocomposites were subjected to TEM, SEM, XRD AND UV vis spectroscopy. TEM showed crystalline nature, and the average particle size was observed to be 42-63 nm and SEM have exhibited well-defined core structure of PPy and the PPy/PCM nanocomposites. XRD patterns of PPy showed the amorphous nature and those of composites showed semicrystalline nature. UV-Vis spectroscopy with Tauc's plot confirmed the band gaps to be in the range of 3.4 – 3.6 eV and hence they may find a place in wide bandgap applications. The UV and visible emissions were observed from the spectrum. DC conductivity studies revealed that PPy/PCM 20 showed maximum conductivity and PPy/PCM 40 was found to be high activation energy. And it is frequency independent at low frequency region and frequency dependent at higher range. The electric Modulus analysis confirmed relaxation of non-Debye type and conductivity obeyed CBH model. Hence these PPy/PCM composites a reproved to be novel materials for application in electric storing device and electrically tunable material which can switch from capacitive to resistive type.

Acknowledgment

The authors gratefully acknowledge the support of this research by the Visveswaraya Technological University (VTU), Belgaum, India. The author is thankful to The Principal, Dr.AIT and B.M.S. College of Engineering, Bengaluru for the co-operation and provision of the necessary facility for synthesis and characterization.

Conflict of Interest

Also we declare that neither of the authors has any personal relationship with other people or organizations that could inappropriately influence this work. Hence there is no conflict of interest.

References

1 Worledge D C, Jeffrey S G , Beasley M R & Geballe T H, *J Appl Phys*, 80 (1996) 5158.
2 Coey J M D, Viret M &Von M S, *Adv Phys,* 48 (1999) 167.
3 Borchert Y, Sonstrom P, Wilhelm M, Borchert H & Baumer M, *J Phys Chem C*, 112 (2008) 3054.
4 Pollert E, Krupicka S & Kuzwicova E, *J Phys Chem Solids*, 43 (1982) 1137.
5 Yan J, Wei T, Shao B, Fan Z Q, Qian W Z , Zhang M L & Wei F, *Carbon*, 48 (2010) 487.
6 Romero A J F, Cascales J J L & Otero T F, *J Phys Chem B*, 109 (2005) 907.
7 Yang C & Liu P, *Ind Eng Chem Res*, 48 (2009) 9498.
8 Wang L X, Li X G &Yang Y L, *React Funct Polym*, 47 (2001) 125.
9 Scott C L, Zhao G J & Pumera M, *Electrochem Commun*, 12 (2010) 1788.
10 Zhao H B, Li L, Yang J & Zhang Y M, *J Power Sources*, 184 (2008) 375.
11 Yang C, Liu P & Zhao Y Q, *Electrochim Acta*, 55 (2010) 6857.
12 Wang Y, Sotzing A G &Weiss A R, *Chem. Mater.* 20 (2008) 2574.
13 Thangadurai V, Huggins R A & Weppner W, *J Solid State Electrochem*, 5 (2001) 531.
14 Zhang J, Manis E &Wilkie C A, *J Nanosci Nanotechnol*, 8 (2008) 1597.
15 Sutar R A & Murugendrappa M V, *J Macromol Sci*, 59 (2020) 821.
16 Kassim A, Sagadavan M, Adzmi F & Mahmud E H N H, *Mater Sci*, 10 (2004) 255.
17 Das B, Kumar S, Chakraborty S, Chakraborty D & Gangopadhyay S , *J Appl Polym Sci*, 69 (1998) 841.

18 Conducting polymers, fundamentals, and applications A Practical Approach, Chandrasekhar P & Ushas A, Corp, Inc, New York, 1st Edn, 1999.
19 Bharathi M, Anuradha K N & Murugendrappa M V, *Elsevier: Mater Today Proc*, 5 (2018) 2818.
20 Chaluvaraju B V, Sangappa K G & Murugendrappa M V, *Polym Sci Ser A*, 57 (2015) 467.
21 Pant H C, Pata M K, Negi S C, Bhatiya A, Vadera S R & Kumar N, *Bull Mater Sci*, 29 (2006) 379.
22 Choudhary M, Islam R Ul, Witcomb M J & Mallick K, *Dalton Trans*, 43 (2014) 6396.
23 Abeles F, North-Holland, Amster-dam, the Netherlands, (1970).
24 Mitchell G R, Davis F J & Legge C H, *Synth Met*, 26 (1988) 247.
25 Kashyap J & Riaz U, *RSC Adv*, 8 (2018) 13218.
26 Patil A O, Heeger A J & Wudl, *Chem Rev*, 88 (1988) 183.
27 Xiao H M & Fu S Y, *Cryst Eng Commun,* 16 (2014) 2097.
28 Achour M E , Droussi A , Medine D, Oueriagli A , Outzourhit A, Belhadj Mohamed A & Zangar H, *Int J Phys Sci*, 6 (2011) 5075.
29 Huang Z, Wang S, Li H, Zhang S & Tan Z, *J Therm Anal Calorim*, 115 (2014) 259.
30 Macedo P B , Moynihan C T & Bose R, *Phys Chem Glass*, 13 (1972) 171.
31 Aaditya V B, Bharathesh B M, Harshitha R, Chaluvaraju B V, Raghavendra U P & Murugendrappa M V, *J Mater Sci: Mater Electron*, 29 (2018) 2848.
32 Naveen K, Bastola N, Kumar S & Ranjan R, *J Mater Sci*, 28 (2017) 10420.
33 Dutta A & Sinha T P, *J Phys Chem Solids*, 67 (2006) 1484.
34 Costa M, Pires G F M, Terezo A J, Grac M P F & Sombra, *J Appl Phys*, 110 (2011) 034107.
35 Sen S, Pramanik P & Choudhary R N P, *Ceram Int*, 33 (2007) 579.
36 Sen S, Choudhary R N P & Pramanik P, *Phys B Condens Matter*, 387 (2007) 56.